Available online at www.sciencedirect.com
ScienceDirect
Journal of Sound and Vibration 311 (2008) 461–472
JOURNAL OF SOUND AND VIBRATION
www.elsevier.com/locate/jsvi

Adaptive positive position feedback for actively absorbing energy in acoustic cavities

M.A. Creasy[a,*], D.J. Leo[a], K.M. Farinholt[b]

[a]Center for Intelligent Material Systems and Structures, Mechanical Engineering, Virginia Tech, Blacksburg, Virginia, USA
[b]Nanosonic Inc., Blacksburg, Virginia, USA

Received 28 February 2007; received in revised form 15 August 2007; accepted 18 September 2007
Available online 5 November 2007

Abstract

A method for adaptive energy absorption in acoustic cavities is presented. The method is based on an adaptive scheme consisting of a self-tuning regulator that has the ability to target multiple modes with a single actuator. The inner control loop of the self-tuning regulator uses positive position feedback in series with a high- and low-pass Butterworth filters for each controlled mode. The outer loop consists of an algorithm that locates the zero frequencies of the collocated signal and uses these values to update the resonance frequency of the positive position feedback filter and the cut-off and cut-on frequencies of the Butterworth filters. Experimental results are provided that show how less than a 10 percent change in the frequencies of the acoustic modes of the experimental setup will cause a non-adaptive controller (using positive position feedback and Butterworth filters) to go unstable, but the self-tuning regulator will maintain stability and continue absorbing energy through a 20 percent change in the frequencies of the acoustic modes.

1. Introduction

Sound properties in acoustic cavities have been the topic of research interest in terms of identifying low-frequency acoustic modes and absorbing acoustic energy in the low-frequency region. Applications of interest have included active control for sound pressure level (SPL) reductions in 1-D acoustic ducts [1–5], the fuselage of passenger jets [6–7], vibration suppression for interior car compartments that reduces the structural acoustic coupling and therefore reduces the interior SPL [8–9], and active control for SPL reductions in payload fairings [10–14]. The boundary conditions of these aforementioned cavities are stiff and cause interior sound waves, along with the associated wave reflections, to produce standing pressure waves with relatively large amplitudes. These standing pressure waves with large amplitudes are considered the acoustic modes of the system and energy absorbed from these acoustic modes will reduce the standing waves amplitudes and reduce the interior SPL.

Passive acoustic devices (Helmholtz resonators and acoustic treatment) help reduce the amplitudes of these standing waves. Helmholtz resonators are effective at reducing these waves in the low-frequency region, but

*Corresponding author.
E-mail address: mcreasy@vt.edu (M.A. Creasy).

0022-460X/$ - see front matter
doi:10.1016/j.jsv.2007.09.013

Nomenclature

a	duct radius
B	speaker magnetic flux density
c	speed of sound
f	frequency (Hz)
$f_{r,N}$	relaxation frequency of molecular nitrogen
$f_{r,0}$	relaxation frequency of molecular oxygen
$\mathbf{F}$	force
F	filter model
g	gain
$\mathbf{G}$	plant model
h	molar concentration of water vapor
$\mathbf{H}$	closed loop plant model
$\mathbf{i}$	current
$\mathbf{k}$	wavenumber (ω/c)
$\mathbf{K}$	PPF filter
$\mathbf{K}_{\mathrm{ppf}}$	sum of multiple filters
l	speaker coil length
L	length
L_e	speaker electrical inductance
m	speaker mass
p_s	atmospheric pressure
p_{s0}	reference atmospheric pressure
$\mathbf{p}$	pressure
Pr	Prandtl number
R	speaker damping
R_e	electrical resistance
s^{-1}	speaker mechanical compliance
s	Laplace variable
S	area
T	temperature
T_0	reference atmospheric temperature
$\mathbf{u}$	mechanical velocity
$\mathbf{U}$	acoustic volume velocity
V_e	external voltage disturbance
V_i	internal voltage disturbance
x	horizontal location on duct
$\mathbf{Z}$	total impedance
$\mathbf{Z}_a$	radiation impedance
$\mathbf{Z}_e$	electrical impedance
$\mathbf{Z}_m$	mechanical impedance
α	absorption coefficient
α_m	molecular thermal relaxation absorption
α_w	wall losses absorption
γ	ratio of specific heats
ζ	damping ratio
ζ_f	filter damping ratio
ξ	modal coordinate
η	coefficient of shear viscosity
ρ	density
ω	frequency (rad/s)
ω_f	filter frequency (rad/s)

Abbreviations

PPF	positive position feedback
STR	self-tuning regulator
SPL	sound pressure level

usually require a resonator for each mode to effectively absorb energy from all the acoustic modes. Acoustic treatment applied to the boundary is most effective at reducing the amplitude of high-frequency modes because the ability of the treatment to absorb energy is dependent on the thickness of the treatment being longer than a quarter of the wavelength of the standing wave [13]. As the thickness of the treatment is increased or more resonators are included in the cavity, the internal volume of the cavity is decreased and additional weight is added to the system, which is usually undesirable for the applications of interest previously mentioned.

Current referenced research has shown that active control has the ability to reduce the noise transmission of sound or absorb interior acoustic energy in the low-frequency region of these cavities. Piezoelectric actuators have been shown to reduce boundary vibrations that couple into the acoustic domain of a car and a fairing and therefore reduces the interior SPL within these cavities [9,15]. Loud speakers have also been shown to work well at absorbing acoustic energy within a duct, the fuselage of a business jet, and a payload fairing [2,3,6,10,16] by driving the loud speaker out of phase with the standing wave of that acoustic mode. The aforementioned control research uses active control that is designed for a system where the acoustic modes are found from system models or measured data. One important aspect usually not addressed in this type of research for these acoustic cavities is system parameter variations and how the robustness of the controller affects the reported SPL reductions.

Large temperature changes, barometric pressure changes, and small geometric changes have the potential to cause changes in the acoustic modes of the system and affect the amount of acoustic energy absorbed by active controllers. Large changes of the system properties can cause an active controller to go unstable. Therefore, an active controller needs to be either robust enough to account for these changes and continue providing sufficient energy absorption or designed using some adaptation scheme to account for system changes. Functional control schemes have some level of robustness to changes. A constant gain feedback system can provide energy absorption over a limited bandwidth [2,3,11], but if more absorption is needed another control scheme will need to be implemented and will probably not be as robust and will require some form of adaptation for large changes. Moon et al. [17,18] present an adaptive control scheme for a finite length duct where the system is changed by removing an endcap. Here, we will consider a similar acoustic cavity that consists of a cylindrical duct with a speaker attached to one end and a varying boundary condition attached to the other end. An impedance model of the system is presented that is used to predict the transfer functions of the system of the pressure measured at any location within the duct over the disturbance voltage input to the speaker. Positive position feedback (PPF) is used in series with high- and low-pass Butterworth filters to actively absorb acoustic energy. An adaptation scheme is presented, consisting of a self-tuning regulator (STR), which allows the control filters to update in real time as the system parameters change. The varying boundary condition is used to show that system changes can cause sufficient variations in the modes to drive a control design unstable unless the adaptation scheme is used to adapt the controller.

2. Analytical model of a finite length duct

The system modeled and used for this research is a cylindrical duct with a varying end cap on one end and a speaker mounted on the other end. Analytical models of this system, which assumes the enclosure to be rigid and smooth with a rigid end cap, have been studied in detail because of the simplicity of the geometry and because plane waves can be assumed in the system at low frequency [19]. Fig. 1 shows a picture and schematic of the system modeled. Three microphones are used to measure the acoustic pressure within the duct at three different points and two different disturbances are used to excite the internal acoustic modes of the duct. The disturbances sources are (1) the speaker attached to one end of the duct, which is also used as the control actuator and (2) two speakers placed externally alongside the duct. The end cap is designed like a piston that can be manually adjusted to change the effective length of the duct cavity. The model of the system obtains the transfer functions of the system where the output is the pressure at any cross-sectional plane of the duct and the input is the voltage into the speaker attached at the end of the duct. The model results shown in this paper for the transfer function outputs are for the cross-sectional planes where the microphones are placed for direct

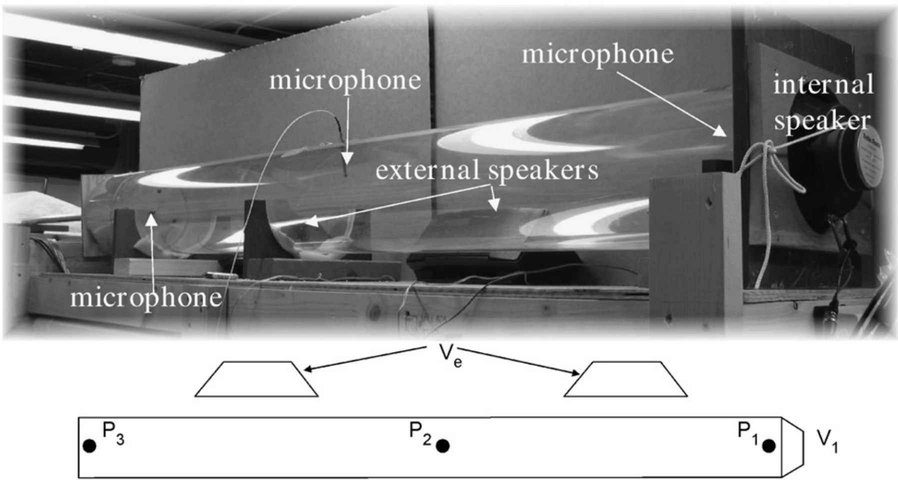

Fig. 1. Photo of the actual test cavity and a schematic of the cavity with defined pressure measurements (P) and disturbances (V) of the system.

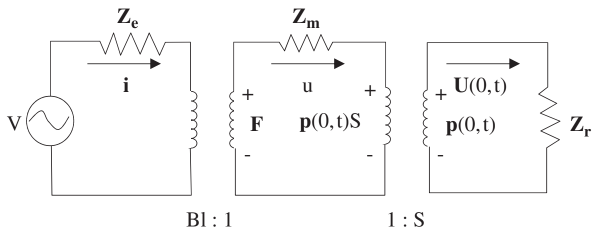

Fig. 2. Combined electromechanical impedance model of the duct with a speaker attached to one end.

comparison of the model to measured data. The model does not predict the transfer functions of the system excited by the external speakers because the transmission path for this disturbance is excluded from the model.

Kinsler et al. [19] show how an impedance model can be used to estimate the internal pressure of a duct. An electromechanical impedance model of the speaker, as shown in Fig. 2 and explained by Beranek [20], can be used to find the total impedance of the speaker accounting for the acoustic, electrical, and mechanical properties. The total impedance of the speaker reduced from the model shown in Fig. 2 is

$$\mathbf{Z}(\omega) = \mathbf{Z}_e(\omega) + \frac{\mathbf{Z}_m(\omega) + S^2\mathbf{Z}_a(\omega)}{(Bl)^2}, \tag{1}$$

where the radiation impedance of the cavity at the speaker edge with the duct can be shown to be [19]

$$\mathbf{Z}_a(\omega) = -j\rho c S \cot(kL) \tag{2}$$

and the mechanical and electrical impedance of the speaker can be shown to be

$$\mathbf{Z}_m(\omega) = R + j(\omega m - s/\omega), \tag{3}$$

$$\mathbf{Z}_e(\omega) = R_e + j\omega L_e, \tag{4}$$

respectively. Now any input voltage can be used with Ohm's law to find an equivalent current into the speaker at the same frequency of the input voltage. The current can be used to calculate an approximate force into the speaker where the force [20] is defined as

$$\mathbf{F}(\omega) = Bl\mathbf{i}(\omega). \tag{5}$$

The acoustic pressure at the surface of the speaker is a function of the calculated force and the radiation and mechanical impedances and is

$$\mathbf{p}(0,\omega) = \frac{\mathbf{F}\mathbf{Z}_a(\omega)}{S(\mathbf{Z}_a(\omega) + \mathbf{Z}_m(\omega))}. \tag{6}$$

The acoustic pressure [19] at any location within the duct as a function of the input frequency is

$$\mathbf{p}(x,\omega) = \mathbf{p}(0,\omega)\frac{\cos[k(L-x)]}{\cos(kL)}. \tag{7}$$

Now, the transfer function between the pressure output and the voltage input of the system at any location within the duct as a function of the disturbance frequency is

$$\mathbf{G}(x,\omega) = \frac{\mathbf{p}(x,\omega)}{V_i(\omega)}. \tag{8}$$

Fig. 3 shows the collocated measured frequency response function of the system compared to the analytical model of the system, defined from Eq. (8), at the same location. This collocated transfer function is the measured pressure at $x = 0.05$ m over the broadband (20–500 Hz) voltage applied to the speaker. The discrepancies between the model and the measured data are the lack of acoustic damping and the fact that amplifier dynamics, which are AC-coupled are neglected in the model. The absence of acoustic damping in the model causes (1) the amplitudes of each mode to be higher and (2) the phase of the model to deviate from the pole/zero relationship (caused by a numerical issue within the code modeling the phase because of the

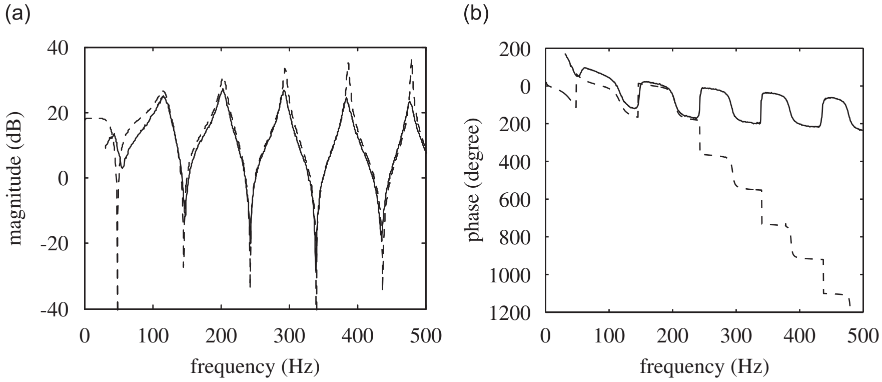

Fig. 3. Comparison of the duct collocated frequency response function (a) magnitude and (b) phase between the measured (—) and modeled (- -) data.

small damping ratio of the zeroes). The absence of the amplifier dynamics causes the deviation between the measured transfer function and the model most noticeably below 100 Hz. This frequency range is where the measured magnitude decreases while the model magnitude levels off and the measured phase is significantly higher than the modeled phase.

To account for these discrepancies, acoustic energy losses and a first-order high-pass Butterworth filter are included in the model to represent the acoustic damping and the amplifier dynamics, respectively. Acoustic energy losses are included by adding an absorption coefficient [19] to the wavenumber making it a complex value

$$\mathbf{k} = k - j\alpha. \tag{9}$$

The absorption coefficient used in this research is the summation of the absorption coefficient for wall losses [19] which is

$$\alpha_w = \frac{1}{ac}\left(\frac{\eta\omega}{2\rho}\right)^{0.5}\left(1 + \frac{\gamma - 1}{\sqrt{Pr}}\right) \tag{10}$$

and the absorption coefficient for molecular thermal relaxation [21] which is

$$\begin{aligned}\alpha_m =& f^2(1.84 \times 10^{-11})\left(\frac{p_s}{p_{s0}}\right)^{-1}\left(\frac{T}{T_0}\right)^{0.5} \\ &+ f^2\left(\frac{T}{T_0}\right)^{-2.5}\left\{\frac{(1.278 \times 10^{-2})e^{(-2239.1/T)}}{f_{r,O} + (f^2/f_{r,O})} + \frac{(1.068 \times 10^{-1})e^{(-3352/T)}}{f_{r,N} + (f^2/f_{r,N})}\right\}.\end{aligned} \tag{11}$$

The relaxation frequency of molecular nitrogen and the relaxation frequency of molecular oxygen [21] are found from

$$f_{r,N} = \frac{p_{\mathrm{s}}}{p_{so}}\left(\frac{T_O}{T}\right)^{1/2}(9 + 280he^{-4.17[(T_O/T)^{1/3}-1]}), \tag{12}$$

$$f_{r,O} = \frac{p_s}{p_{so}}\left(24 + 40400h\frac{(0.02 + h)}{(0.391 + h)}\right), \tag{13}$$

respectively. The audio amplifier used to drive the speaker is modeled with the first-order high-pass Butterworth filter

$$F(s) = \frac{s}{s + 300}. \tag{14}$$

This filter increases the low-frequency model phase by 90° due to the zero in the numerator and gives the model a 20 dB per decade roll-on below 50 Hz and levels off after 50 Hz.

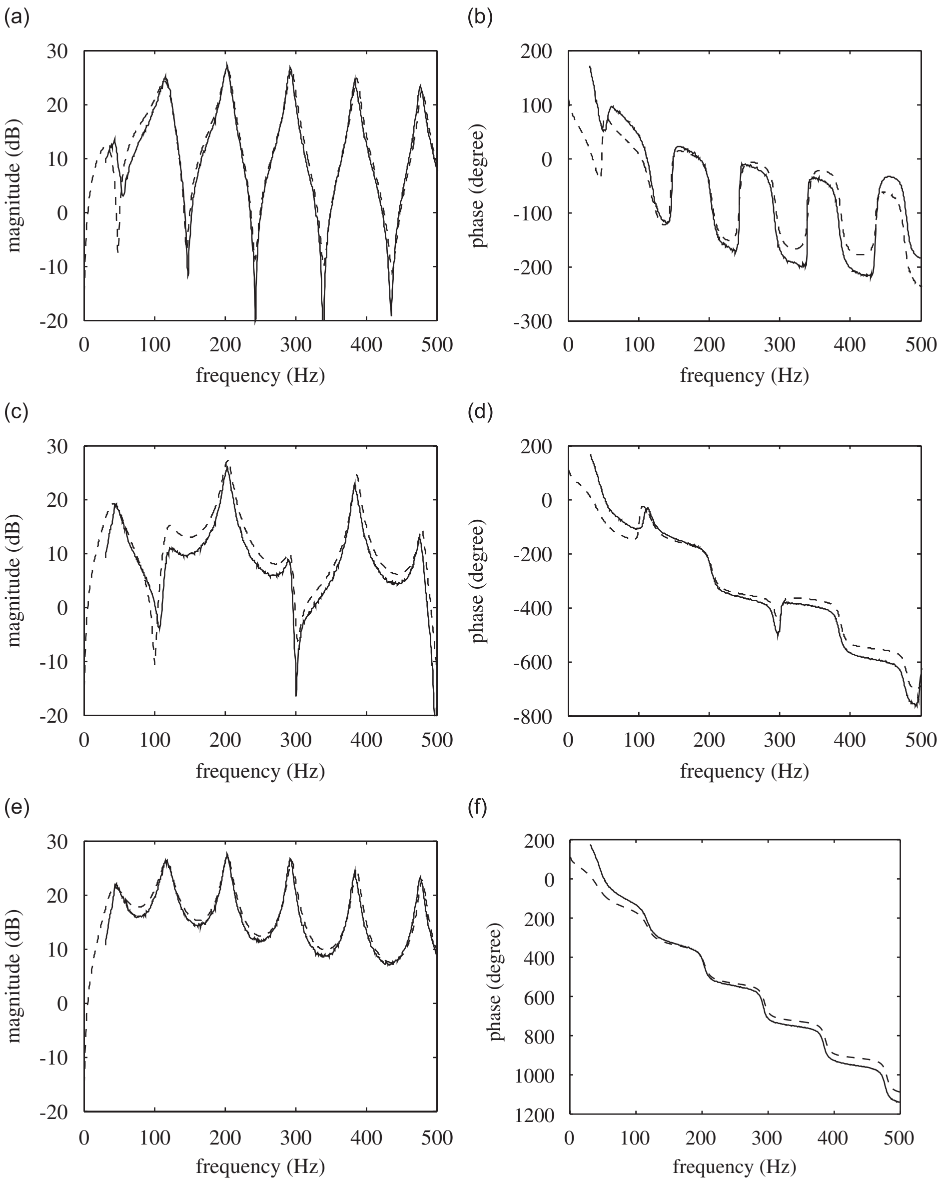

Fig. 4. Duct frequency response function comparison between measured (—) and modeled (- -) data for the three measurement locations shown in Fig. 1: (a) collocated (P_1/V_i) magnitude, (b) collocated (P_1/V_i) phase, (c) P_2/V_i magnitude, (d) P_2/V_i phase, (e) P_3/V_i magnitude, and (f) P_3/V_i phase.

The measured transfer functions of the duct at the three microphone locations are compared with the model results at the same locations. Fig. 4 shows the measured frequency response functions of the system (at $x = 0.05$, 0.97, and 1.80 m) compared with the model of the system including the acoustic energy losses and amplifier dynamics. All three frequency response functions show that the model follows the magnitude and phase trends of the measured transfer functions well in this frequency region. Table 1 contains all the constants and values used to obtain this analytical model.

3. Control development

Positive position feedback is the controller chosen for this research in order to absorb acoustic energy from within the duct. Fanson and Caughey [22] describe positive position feedback controllers by first defining a

Table 1
Duct, speaker, and air constants

	Symbol	Value	Units
Duct constants			
Duct radius	a	0.1016	m
Duct cross sectional area	S	0.0324	m^2
Duct length	L	1.83	m
Speaker constants			
Speaker dynamic mass	m_s	18.38	g
Speaker mechanical compliance	s^{-1}	1174.63	μm/N
Speaker electrical resistance	R_e	6.6	Ω
Speaker electrical inductance	L_e	0.93	mH
Speaker damping (assumed critical damping)	R	7.91	Ns/m
Speaker magnetic flux density and wire length	Bl	6.77	T m
Air constants			
Air density	ρ	1.1877	kg/m^3
Air speed of sound	c	345.25	m/s
Atmospheric pressure	p_s	100,680	Pa
Reference atmospheric pressure	p_{s0}	101,325	Pa
Temperature	T	295.15	K
Reference atmospheric temperature	T_0	273.15	K
Relaxation frequency of molecular oxygen	$f_{r,0}$	41,225	Hz
Relaxation frequency of molecular nitrogen	$\mathrm{f}_{r,N}$	399.19	Hz
Molar concentration of water vapor	h	1.31	Percent
Prandtl number	Pr	0.710	Unitless
Coefficient of shear viscosity	η	1.88×10^5	Pa s
Ratio of specific heats	γ	1.402	Unitless

second-order equation for the modal coordinate of the system as

$$\ddot{\xi} + 2\zeta\omega\dot{\xi} + \omega^2\xi = g\omega^2\eta \tag{15}$$

and a second-order equation for the filter coordinate as

$$\ddot{\eta} + 2\zeta_f\omega_f\dot{\eta} + \omega_f^2\eta = \omega_f^2\xi. \tag{16}$$

A transfer function of the positive position feedback filter then takes the form

$$K(s) = \frac{g\omega_f^2}{s^2 + 2\zeta_f\omega_f s + \omega_f^2} \tag{17}$$

and shows that the filter adds two poles to the system for each positive position feedback filter used.

The intent of using the positive position feedback filter in this research is to add damping to a particular mode in the system where the positive position feedback filter is designed and this filter has been used by other researchers in vibration suppression and SPL reduction [22–24]. Fig. 5 contains a bode plot of a sample positive position feedback filter in order to show the frequency characteristics of the filter where the magnitude is normalized to 0 dB and the frequency is normalized to the resonance frequency of the positive position feedback filter. The large phase shift from 0° to −180° at the resonance frequency of the filter causes the filter to be out of phase with the input of a system over the frequency band where this phase change is occurring. When the output of the system is fed-back through this filter and the result is added to the input, the amplitude of the output is reduced in the frequency band where the phase change is occurring. Goh [23] and McEver [24] derived procedures for optimizing the variables of the positive position feedback filter.

One problem linked with the filter is the flat magnitude response at frequencies below the filter resonance frequency. This flat response can cause low-frequency spillover as higher modes are controlled because the phase of the filter is close to zero and will therefore be in phase with the output of the system. The positive position feedback filter works well at low frequencies because above the resonance frequency, the magnitude

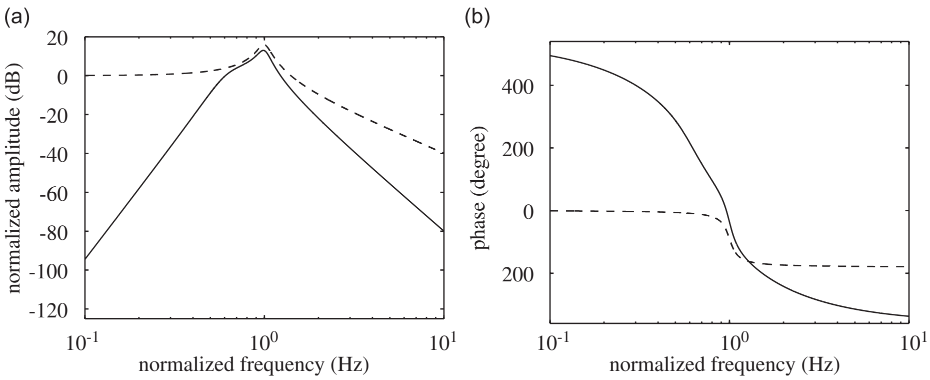

Fig. 5. Bode plots: (a) magnitude and (b) phase of positive position feedback filter (- -) and combined positive position feedback and Butterworth filters (—).

of the filter rolls-off at 40 dB per decade and high-frequency dynamics of the system remain unaffected by the filter. Modeling and testing of this system showed that using one positive position feedback filter to damp a single mode caused very little spillover into lower modes, however when multiple positive position feedback filters are added to a system to control multiple modes, the spillover effect into lower modes increases significantly. Bisnette et al. [1] used velocity feedback filters that introduced a zero in the transfer function of Eq. (17). This zero causes the magnitude to roll-up at 20 dB per decade frequencies below the filter resonance but reduces the roll-off at higher frequencies to 20 dB per decade. Smith and Vipperman [5] show that high-order Butterworth filters can be used as a band-pass filter for multimodal control.

The spillover effect of the positive position feedback filters is reduced with the use of Butterworth filters. A sixth-order high-pass and a second-order low-pass Butterworth filters are used in series with the positive position feedback filter to reduce the low-frequency spillover and increase the high frequency roll-off. Fig. 5 also contains a bode plot of the positive position feedback filter combined in series with a sixth-order high-pass and a second-order low-pass Butterworth filter. The new filter increases the high-frequency roll-off to 80 dB per decade, provides a roll-on of 120 dB per decade at low frequency, and maintains a phase change at the resonance of the filter although the phase change is occurring from 90° to -90°. The positive position feedback design optimization procedures, previously referenced, do not account for these additional dynamics, so simulations and experiments are used to approximate optimized filter properties.

The model of the duct is used to simulate control on the system in order to see the effectiveness of the controller. The simulated closed-loop transfer function with a positive compensator in the feedback loop [25] is defined as

$$H(s) = \frac{G(s)}{1 - G(s)K_{\text{ppf}}(s)}, \tag{18}$$

where s can be replaced with $j\omega$ to estimate the closed-loop transfer function in terms of its magnitude and phase. The optimized filter parameter settings are found from both simulations of the closed-loop system where the plant G is found from Eq. (8), and from experimental work. The results of the simulations and experiments indicate that a band-pass filter, consisting of the two Butterworth filters, around the mode being controlled will minimize spillover into higher and lower modes. Therefore, the cut-on frequency of the high-pass Butterworth filter should be set to the frequency of the zero preceding the controlled mode and the frequency of the low-pass Butterworth filter should be set to the frequency of the zero following the mode. The damping ratio of the positive position feedback filter should be set to a value approximately an order of magnitude higher than the damping ratio of the mode being controlled. The resonance of the positive position feedback filter should be set close to the frequency of the zero following the mode which is the same value that is used to set the low-pass Butterworth filter. The gain for each set of filters can be found by incrementally increasing the gains using a top/down approach, starting at the highest mode to be controlled and working down to the lowest.

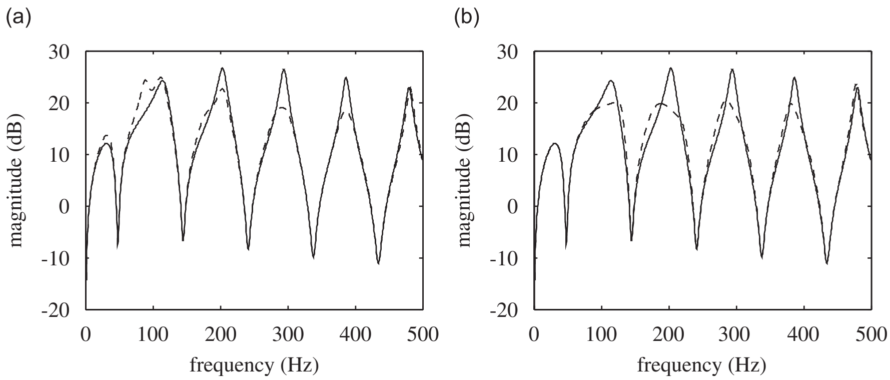

Fig. 6. Magnitude plots of the duct model (—) overlaid with magnitude plots of the simulated controlled system (- -) using only (a) positive position feedback control filters and (b) combined positive position feedback and Butterworth filters.

Positive position feedback filters and positive position feedback filters combined with Butterworth filters are designed and tuned for the second through fifth modes of the model. Fig. 6 shows the collocated magnitude results of both control simulations overlaid on the model of the system. The plot where only positive position feedback filters are used shows how the third through fifth modes amplitudes have been reduced, but the amplitudes for the first and second modes have increased. The plot where the combined positive position feedback and Butterworth filters are used shows little spillover into the first and second modes' amplitudes. Both plots show that the amplitude of the sixth mode is maintained level without any significant increase showing little to no spillover into higher modes.

4. Self-tuning regulator and algorithm

The robustness of the controller consisting of the combined positive position feedback and Butterworth filters is assessed by changing the length of the duct model where control is simulated. Simulations for the duct with an increase and decrease of length by 5 percent show that the system remains stable, but the magnitude reductions seen in Fig. 6 are significantly effected. Fig. 7 shows these simulated results for the duct length increase and decrease compared to the model of the system without control and without length changes. The simulations show the modes shift higher and lower in frequency for the decrease and increase of duct length, respectively, but each simulation shows that the magnitude of at least one of the controlled modes is increased over the magnitude of the system without control. These results show that small variations can significantly affect the amplitude reductions of the active controller and could potentially increase the interior SPL.

To increase the robustness of the controller a self-tuning regulator is designed to update the control parameters as the system changes. A self-tuning regulator is described as having two loops: (1) the conventional controller loop with varying parameters and (2) an identifying and control algorithm loop that identifies the system and changes the varying parameters of the conventional controller [26]. For this work, the collocated microphone signal is used as the feedback signal for both of these loops. Fig. 8 shows a schematic of the self-tuning regulator control block diagram used in this research. The conventional controller loop is the loop that contains the K_{ppf} block and contains a parameter varying transfer function of the combined positive position feedback and Butterworth filters. The parameter variations can be the gain, damping, or resonance frequency of the positive position feedback filter; the cut-on or cut-off frequencies of the Butterworth filters; or any combination of these parameters and can be updated in real time. The control algorithm loop determines the varying parameters for the filters. For this research simulations were used to determine the gain and damping values of the positive position feedback filters and the control algorithm loop was used to determine the positive position feedback resonance frequency and the Butterworth filter's cut-on and cut-off frequencies. Since these values were determined by the zeros of the collocated signal as previously explained, the time data of the collocated pressure signal is transformed to frequency data. A buffer is used to accumulate the collocated pressure measurements to perform the fast Fourier transform (FFT) of the data in real time.

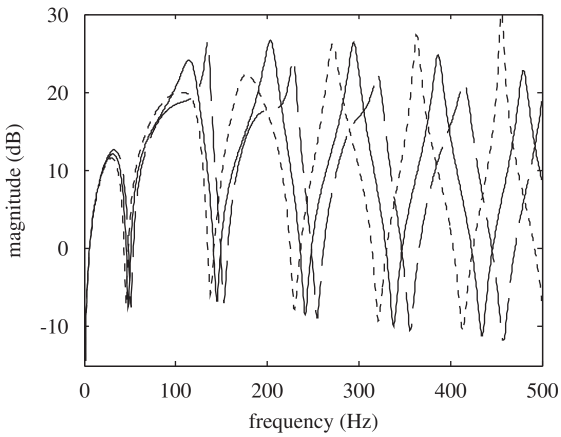

Fig. 7. Magnitude plots of the duct model (——) over laid with magnitude plots of the simulated controlled system with the length shortened by 5 percent (– –) and with the length increased by 5 percent (- -).

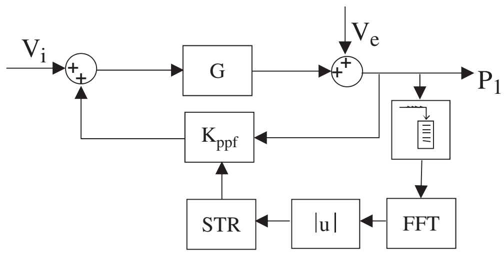

Fig. 8. Self-tuning regulator block diagram used in this research.

The magnitude of this FFT data is sent to an algorithm that searches for the minimum magnitude values and the associated frequency values and these frequency values coincide with the zeros of the system. The frequency values of the zeros are used to update the varying parameters of the transfer functions as explained.

Adaptation speed is not a priority to account for rate changes or step changes in the system. The control algorithm loop of the self-tuning regulator takes about 0.4 s running at 5000 Hz to capture 2048 data points, perform the FFT, extract the zero frequency values from the collocated signal, and update the parameter varying transfer functions. Owing to computational errors in the FFT and the coded algorithm, a running average of the systems zeros keeps the system from going unstable. For this research, a continuous running average of 20 zero frequency values are stored and averaged to maintain stability. The controller is not optimized for the minimum number of averages needed to maintain stability and the total time to update the controller with the running average of 20 data points is about 8 s.

5. Experimental results

Experiments are performed on the varying length duct. Testing shows that as the duct length is changed from an initial 1.83 to 1.52 m in length, the second through sixth modes' frequencies change by more than 20 percent from the original values and the damping remains relatively constant as shown in Table 2. The frequency for each pair of poles at each mode is found from the associated frequency of the maximum magnitude of each mode from the transfer function of the collocated measured data. The frequency of each pair of zeros from the collocated data is found from the associated frequency of the minimum magnitude between the modes. The damping ratios are found from the *3-dB down point* [27] rule. The first mode is dominated by the first natural frequency of the speaker and is therefore not affected by the system changes in the same manner as the other modes.

Table 2
Frequencies of the poles and zeros of the duct length extremes

1.83 m duct						
Poles (Hz)	43.8	115.6	203.1	292.5	383.8	476.9
Damping ratio	0.15	0.06	0.02	0.01	0.01	0.01
Zeros (Hz)	56.3	148.1	243.1	339.4	435.6	531.9
1.52 m duct						
Poles (Hz)	39.4	142.5	243.8	353.1	462.5	573.8
Damping ratio	0.16	0.06	0.02	0.01	0.01	0.02
Zeros (Hz)	56.3	182.5	297.5	413.1	528.1	647.5
Mode changes (percentage)						
	−10.0	23.2	20.0	20.7	20.5	20.3

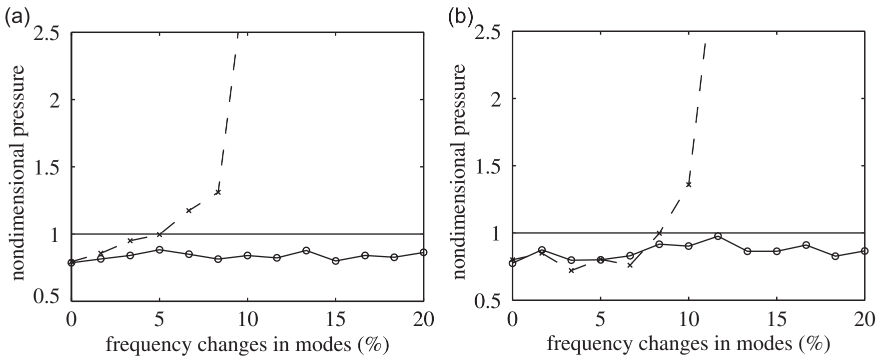

Fig. 9. Non-dimensional pressure reductions of the duct with (a) internal and (b) external system disturbances as the frequencies of the modes are changed by 20 percent for the adaptive (—) and non-adaptive (- -) scenarios.

Non-adaptive and adaptive control tests are performed with the duct in two different test scenarios. The first test scenario uses the internal speaker as the disturbance and the control actuator and the second test scenario uses the external speakers as the disturbance source and the internal speaker as the control actuator. Measurements are made at 1 in increments after at least a 10 s delay for each increment as the duct length is changed from 1.83 to 1.52 m. Non-adaptive tests are stopped after excessive vibrations and noise is measured, indicating near instabilities.

Fig. 9 shows the test results from both scenarios. The abscissas of the plots are the percent changes of the frequencies of the modes and the ordinates of the plots are the non-dimensional pressure of the system. The non-dimensional pressure is the controlled system pressure over the baseline non-controlled system pressure of that particular duct length. Therefore, any non-dimensional pressure above unity would actually be increasing the internal SPL of the system. The pressures used are the average pressure found from the three microphone measurement locations over the 50–500 Hz range. These plots show that the non-adaptive controller increases the internal average pressure in the low-frequency region after the duct length is reduced by 5 and 8 percent for the internal and external disturbances, respectively. The adaptive controller remains stable for the entire 20 percent change and decreases the internal average pressure over the entire change.

6. Summary and conclusions

The reported experimental work and simulations show that small changes in an acoustic cavity can cause large variations in the frequencies of the cavity's acoustic modes. Positive position feedback control has been shown to work well in absorbing energy from multiple modes using a single controlled speaker. Adding Butterworth filters in series with the positive position feedback filter has been shown to virtually eliminate the low-frequency spillover inherent with positive position feedback control. The simulations show that small boundary variations can detune an active controller and experimental results show that less than a 10 percent change in the frequencies of the acoustic modes can cause an actively controlled system to go unstable. Using a self-tuning regulator to track and update the filter parameters is shown to maintain stability of an active controller and absorb acoustic energy through a 20 percent change in the frequencies of the acoustic modes.

References

[1] J.B. Bisnette, A.K. Smith, J.S. Vipperman, D.D. Bundy, Active noise control using phase-compensated, damped resonant filters, *Journal of Vibration and Acoustics* 128 (2) (2006) 148–155.

[2] R.L. Clark, D.G. Cole, K.D. Framption, Phase compensation for feedback control of enclosed sound fields, *Journal of Sound and Vibration* 195 (5) (1996) 701–718.

[3] R.L. Clark, D.G. Cole, Active damping of enclosed sound fields through direct rate feedback control, *Journal of the Acoustical Society of America* 97 (3) (1995) 1710–1716.

[4] H.R. Pota, A.G. Kellar, Modeling and control of acoustic ducts, *Journal of Vibration and Acoustics* 123 (1) (2001) 2–9.

[5] A.K. Smith, J.S. Vipperman, Adaptive resonant mode acoustic controller, *IMECE2005-89279, ASME IMECE 2005*, Orlando, FL, November 5–11.

[6] R.L. Clark, G.P. Gibbs, Analysis, testing, and control of a reverberant sound field within the fuselage of a business jet, *Journal of the Acoustical Society of America* 105 (5) (1999) 2277–2286.

[7] S.A. Lane, R.L. Clark, S.C. Southward, Active control of low frequency modes in an aircraft fuselage using spatially weighted arrays, *Journal of Vibration and Acoustics* 122 (3) (2000) 227–234.

[8] S.W. Kang, J.M. Lee, S.H. Kim, Structural–acoustic coupling analysis of the vehicle passenger compartment with the roof, air-gap, and trim boundary, *Journal of Vibration and Acoustics* 122 (3) (2000) 196–202.

[9] C.K. Song, J.K. Hwang, J.M. Lee, J.K. Hedrick, Active vibration control for structural–acoustic coupling system of a 3-D vehicle cabin model, *Journal of Sound and Vibration* 267 (4) (2003) 851–865.

[10] B.K. Henderson, S.A. Lane, J. Gussy, S. Griffin, K.M. Farinholt, Development of an acoustic actuator for launch vehicle noise reduction, *Journal of the Acoustical Society of America* 111 (1) (2002) 174–179.

[11] J.D. Kemp, R.L. Clark, Noise reduction in a launch vehicle fairing using actively controlled loudspeakers, *Journal of the Acoustical Society of America* 113 (4) (2003) 1986–1994.

[12] S.A. Lane, R.L. Clark, Dissipative feedback control of a reverberant enclosure using a constant volume velocity source, *Journal of Vibration and Acoustics* 120 (4) (1998) 833–1008.

[13] S.A. Lane, M. Johnson, C. Fuller, A. Charpentier, Active control of payload fairing noise, *Journal of Sound and Vibration* 290 (3–5) (2006) 794–819.

[14] S.A. Lane, J.D. Kemp, S. Griffin, R.L. Clark, Active acoustic control of a rocket fairing using spatially weighted transducer arrays, *Journal of Spacecraft and Rockets* 38 (1) (2001) 112–119.

[15] S.A. Lane, S. Griffin, D. Leo, Active structural–acoustic control of composite fairings using single-crystal piezoelectric actuators, *Smart Materials & Structures* 12 (1) (2003) 96–104.

[16] S.A. Lane, R.L. Clark, Improving loudspeaker performance for active noise control applications, *Journal of the Audio Engineering Society* 46 (6) (1998) 508–519.

[17] S.M. Moon, R.L. Clark, D.G. Cole, The recursive generalized predictive feedback control: theory and experiments, *Journal of Sound and Vibration* 279 (1–2) (2005) 171–199.

[18] S.M. Moon, D.G. Cole, R.L. Clark, Real-time implementation of adaptive feedback and feedforward generalized predictive control algorithm, *Journal of Sound and Vibration* 294 (1–2) (2006) 82–96.

[19] L.E. Kinsler, A.R. Frey, A.B. Coppens, J.V. Sanders, *Fundamentals of Acoustics*, fourth ed., Wiley, New York, 2000.

[20] L.L. Beranek, *Acoustics*, American Institute of Physics, Woodbury, New York, 1996.

[21] H.E. Bass, L.C. Sutherland, A.J. Zuckerwar, Atmospheric absorption of sound: update, *Journal of the Acoustical Society of America* 88 (4) (1990) 2019–2021.

[22] J.L. Fanson, T.K. Caughey, Positive position feedback control for large space structures, *American Institute of Aeronautics and Astronautics Journal* 28 (4) (1990) 717–724.

[23] C.J. Goh, Analysis and Control of Quasi Distributed Parameter Systems, PhD Dissertation, California Institute of Technology, 1983.

[24] M. McEver, D.J. Leo, Autonomous vibration suppression using on-line pole-zero identification, *Journal of Vibration and Acoustics* 123 (4) (2001) 487–495.

[25] R.C. Dorf, R.H. Bishop, *Modern Control Systems*, ninth ed., Prentice-Hall, Upper Saddle River, NJ, 2001.

[26] S. Sastry, M. Bodson, *Adaptive Control: Stability, Convergence, and Robustness*, Prentice-Hall, Englewood Cliffs, NJ, 1989.

[27] D.J. Inman, *Engineering Vibration*, second ed., Prentice-Hall, Upper Saddle River, NJ, 2001.